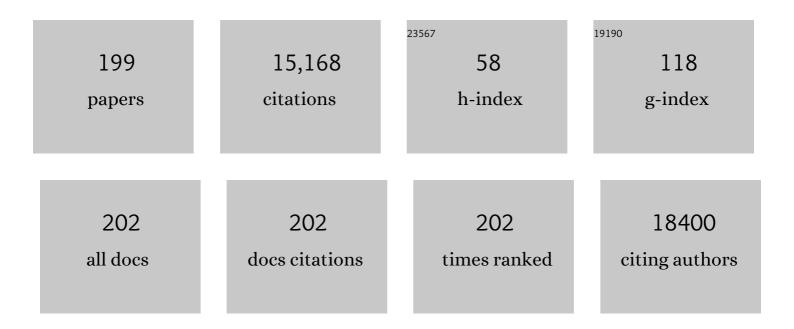
List of Publications by Year in descending order

Source: https://exaly.com/author-pdf/5993468/publications.pdf Version: 2024-02-01



Ιιινννι Ζητι

#	Article	IF	CITATIONS
1	Graphene Oxideâ^MnO <sub>2</sub> Nanocomposites for Supercapacitors. ACS Nano, 2010, 4, 2822-2830.	14.6	1,983
2	Grapheneâ^'Metal Particle Nanocomposites. Journal of Physical Chemistry C, 2008, 112, 19841-19845.	3.1	1,466
3	Bioinspired Effective Prevention of Restacking in Multilayered Graphene Films: Towards the Next Generation of Highâ€Performance Supercapacitors. Advanced Materials, 2011, 23, 2833-2838.	21.0	954
4	Highâ€Performance 2.6 V Aqueous Asymmetric Supercapacitors based on In Situ Formed Na <sub>0.5</sub> MnO <sub>2</sub> Nanosheet Assembled Nanowall Arrays. Advanced Materials, 2017, 29, 1700804.	21.0	526
5	One-Step Synthesis of Grapheneâ^'Cobalt Hydroxide Nanocomposites and Their Electrochemical Properties. Journal of Physical Chemistry C, 2010, 114, 11829-11834.	3.1	313
6	Preparation of NiO nanoparticles and their catalytic activity in the thermal decomposition of ammonium perchlorate. Thermochimica Acta, 2005, 437, 106-109.	2.7	298
7	Deposition of Co3O4 nanoparticles onto exfoliated graphite oxide sheets. Journal of Materials Chemistry, 2008, 18, 5625.	6.7	290
8	Reduction of nitrophenols to aminophenols under concerted catalysis by Au/g-C3N4 contact system. Applied Catalysis B: Environmental, 2017, 202, 430-437.	20.2	253
9	Highly dispersed CuO nanoparticles prepared by a novel quick-precipitation method. Materials Letters, 2004, 58, 3324-3327.	2.6	243
10	2D Fe-containing cobalt phosphide/cobalt oxide lateral heterostructure with enhanced activity for oxygen evolution reaction. Nano Energy, 2019, 56, 109-117.	16.0	223
11	Ag/g-C <sub>3</sub> N <sub>4</sub> catalyst with superior catalytic performance for the degradation of dyes: a borohydride-generated superoxide radical approach. Nanoscale, 2015, 7, 13723-13733.	5.6	216
12	Synthesis of amphiphilic graphite oxide. Carbon, 2008, 46, 386-389.	10.3	197
13	Covalently coupled hybrid of graphitic carbon nitride with reduced graphene oxide as a superior performance lithium-ion battery anode. Nanoscale, 2014, 6, 12555-12564.	5.6	194
14	Decorating graphene oxide with CuO nanoparticles in a water–isopropanol system. Nanoscale, 2010, 2, 988.	5.6	175
15	Ternary manganese ferrite/graphene/polyaniline nanostructure with enhanced electrochemical capacitance performance. Journal of Power Sources, 2014, 266, 384-392.	7.8	169
16	Shape-Controlled Synthesis of One-Dimensional MnO <sub>2</sub> via a Facile Quick-Precipitation Procedure and its Electrochemical Properties. Crystal Growth and Design, 2009, 9, 4356-4361.	3.0	167
17	Perfluoroalkyl-Functionalized Covalent Organic Frameworks with Superhydrophobicity for Anhydrous Proton Conduction. Journal of the American Chemical Society, 2020, 142, 14357-14364.	13.7	167
18	Self-standing porous LiMn 2 O 4 nanowall arrays as promising cathodes for advanced 3D microbatteries and flexible lithium-ion batteries. Nano Energy, 2016, 22, 475-482.	16.0	166

#	Article	IF	CITATIONS
19	Reduced graphene oxide decorated with CuO–ZnO hetero-junctions: towards high selective gas-sensing property to acetone. Journal of Materials Chemistry A, 2014, 2, 18635-18643.	10.3	150
20	Optimizing Hybridization of 1T and 2H Phases in MoS <sub>2</sub> Monolayers to Improve Capacitances of Supercapacitors. Materials Research Letters, 2015, 3, 177-183.	8.7	149
21	In situ fabrication of novel Z-scheme Bi 2 WO 6 quantum dots/g-C 3 N 4 ultrathin nanosheets heterostructures with improved photocatalytic activity. Applied Surface Science, 2015, 355, 379-387.	6.1	141
22	Yolk–shell-structured MnO <sub>2</sub> microspheres with oxygen vacancies for high-performance supercapacitors. Journal of Materials Chemistry A, 2018, 6, 1601-1611.	10.3	135
23	Iron-Cluster-Directed Synthesis of 2D/2D Fe–N–C/MXene Superlattice-like Heterostructure with Enhanced Oxygen Reduction Electrocatalysis. ACS Nano, 2020, 14, 2436-2444.	14.6	130
24	From Graphene to Metal Oxide Nanolamellas: A Phenomenon of Morphology Transmission. ACS Nano, 2010, 4, 6212-6218.	14.6	116
25	Design and fabrication of highly open nickel cobalt sulfide nanosheets on Ni foam for asymmetric supercapacitors with high energy density and long cycle-life. Journal of Power Sources, 2018, 378, 31-39.	7.8	115
26	Preparation and characterization of perovskite LaFeO3 nanocrystals. Materials Letters, 2006, 60, 1767-1770.	2.6	110
27	Recent advances on multi-component hybrid nanostructures for electrochemical capacitors. Journal of Power Sources, 2015, 294, 31-50.	7.8	107
28	Cobalt Sulfide/Graphene Composite Hydrogel as Electrode for High-Performance Pseudocapacitors. Scientific Reports, 2016, 6, 21717.	3.3	105
29	Self-Assembly of Ir-Based Nanosheets with Ordered Interlayer Space for Enhanced Electrocatalytic Water Oxidation. Journal of the American Chemical Society, 2022, 144, 2208-2217.	13.7	103
30	NbS <sub>2</sub> Nanosheets with M/Se (M = Fe, Co, Ni) Codopants for Li <sup>+</sup> and Na <sup>+</sup> Storage. ACS Nano, 2017, 11, 10599-10607.	14.6	95
31	Dense films formed during Ti anodization in NH4F electrolyte: Evidence against the field-assisted dissolution reactions of fluoride ions. Electrochemistry Communications, 2020, 111, 106663.	4.7	95
32	Recent development and applications of electrical conductive MOFs. Nanoscale, 2021, 13, 485-509.	5.6	95
33	Strong Chemical Interaction between Lithium Polysulfides and Flameâ€Retardant Polyphosphazene for Lithium–Sulfur Batteries with Enhanced Safety and Electrochemical Performance. Advanced Materials, 2021, 33, e2007549.	21.0	93
34	Recent advances in graphene-based hybrid nanostructures for electrochemical energy storage. Nanoscale Horizons, 2016, 1, 340-374.	8.0	92
35	Switchable encapsulation of polysulfides in the transition between sulfur and lithium sulfide. Nature Communications, 2020, 11, 845.	12.8	92
36	Depositing ZnO nanoparticles onto graphene in a polyol system. Materials Chemistry and Physics, 2011, 125, 617-620.	4.0	91

Јимwи Ζни

#	Article	IF	CITATIONS
37	Cadmium Sulfide–Ferrite Nanocomposite as a Magnetically Recyclable Photocatalyst with Enhanced Visible-Light-Driven Photocatalytic Activity and Photostability. Industrial & Engineering Chemistry Research, 2013, 52, 17126-17133.	3.7	90
38	Fabrication of a low defect density graphene-nickel hydroxide nanosheet hybrid with enhanced electrochemical performance. Nano Research, 2012, 5, 11-19.	10.4	89
39	Graphene-based 3D composite hydrogel by anchoring Co3O4 nanoparticles with enhanced electrochemical properties. Physical Chemistry Chemical Physics, 2013, 15, 12940.	2.8	89
40	Salt-Assisted Synthesis of 3D Porous g-C <sub>3</sub> N <sub>4</sub> as a Bifunctional Photo- and Electrocatalyst. ACS Applied Materials & amp; Interfaces, 2019, 11, 27226-27232.	8.0	89
41	Rambutanâ€Like Hybrid Hollow Spheres of Carbon Confined Co <sub>3</sub> O <sub>4</sub> Nanoparticles as Advanced Anode Materials for Sodiumâ€Ion Batteries. Advanced Functional Materials, 2019, 29, 1807377.	14.9	89
42	Needle-shaped nanocrystalline CuO prepared by liquid hydrolysis of Cu(OAc)2. Materials Science & Engineering A: Structural Materials: Properties, Microstructure and Processing, 2004, 384, 172-176.	5.6	85
43	Preparation and characterization of Ln2Zr2O7 (Ln=La and Nd) nanocrystals and their photocatalytic properties. Journal of Alloys and Compounds, 2008, 465, 280-284.	5.5	85
44	Synthesis and characterization of graphene paper with controllable properties via chemical reduction. Journal of Materials Chemistry, 2011, 21, 14631.	6.7	85
45	Fabrication of α-Fe2O3@graphene nanostructures for enhanced gas-sensing property to ethanol. Applied Surface Science, 2014, 292, 278-284.	6.1	85
46	2D/2D heterostructures of nickel molybdate and MXene with strong coupled synergistic effect towards enhanced supercapacitor performance. Journal of Power Sources, 2019, 414, 540-546.	7.8	83
47	TiO2 nanotube arrays with a volume expansion factor greater than 2.0: Evidence against the field-assisted ejection theory. Electrochemistry Communications, 2020, 114, 106717.	4.7	82
48	MnO2 based sandwich structure electrode for supercapacitor with large voltage window and high mass loading. Chemical Engineering Journal, 2019, 368, 525-532.	12.7	72
49	Synthesis of flower-like CuO nanostructures via a simple hydrolysis route. Materials Letters, 2007, 61, 5236-5238.	2.6	71
50	One-step synthesis of low defect density carbon nanotube-doped Ni(OH)2 nanosheets with improved electrochemical performances. RSC Advances, 2011, 1, 484.	3.6	70
51	Synthesis of ZnO–Ag Hybrids and Their Gas-Sensing Performance toward Ethanol. Industrial & Engineering Chemistry Research, 2015, 54, 8947-8953.	3.7	70
52	Catalytic Activity of Nanometer-Sized CuO/Fe <sub>2</sub> O <sub>3</sub> on Thermal Decompositon of AP and Combustion of AP-Based Propellant. Combustion Science and Technology, 2010, 183, 154-162.	2.3	66
53	Self-assembled hydrothermal synthesis for producing a MnCO3/graphene hydrogel composite and its electrochemical properties. RSC Advances, 2013, 3, 4400.	3.6	66
54	Synthesis of Cu-Fe3O4@graphene composite: A magnetically separable and efficient catalyst for the reduction of 4-nitrophenol. Materials Research Bulletin, 2014, 57, 190-196.	5.2	65

#	Article	IF	CITATIONS
55	Two-dimensional organic–inorganic superlattice-like heterostructures for energy storage applications. Energy and Environmental Science, 2020, 13, 4834-4853.	30.8	64
56	In-situ synthesis of MnCo2O4.5 nanosheets on reduced graphene oxide for a great promotion in the thermal decomposition of ammonium perchlorate. Applied Surface Science, 2019, 483, 496-505.	6.1	63
57	Pressure difference-induced synthesis of P-doped carbon nanobowls for high-performance supercapacitors. Chemical Engineering Journal, 2020, 385, 123858.	12.7	60
58	Identifying electrocatalytic activity and mechanism of Ce1/3NbO3 perovskite for nitrogen reduction to ammonia at ambient conditions. Applied Catalysis B: Environmental, 2021, 280, 119419.	20.2	60
59	Construction of triple-shelled hollow nanostructure by confining amorphous Ni-Co-S/crystalline MnS on/in hollow carbon nanospheres for all-solid-state hybrid supercapacitors. Chemical Engineering Journal, 2021, 416, 129500.	12.7	60
60	Biomimetic assembly to superplastic metal–organic framework aerogels for hydrogen evolution from seawater electrolysis. Exploration, 2021, 1, 217.	11.0	59
61	Synthesis of Bi nanowire networks and their superior photocatalytic activity for Cr( <scp>vi</scp> ) reduction. Nanoscale, 2014, 6, 10062-10070.	5.6	57
62	Ultrathin molybdenum disulfide/carbon nitride nanosheets with abundant active sites for enhanced hydrogen evolution. Nanoscale, 2018, 10, 1766-1773.	5.6	57
63	Atomic-scale regulation of anionic and cationic migration in alkali metal batteries. Nature Communications, 2021, 12, 4184.	12.8	57
64	One-pot hydrothermal route to synthesize the ZnIn2S4/g-C3N4 composites with enhanced photocatalytic activity. Journal of Materials Science, 2015, 50, 8142-8152.	3.7	56
65	A safe and efficient liquid-solid synthesis for copper azide films with excellent electrostatic stability. Nano Energy, 2019, 66, 104135.	16.0	56
66	CuO nanocrystals with controllable shapes grown from solution without any surfactants. Materials Chemistry and Physics, 2008, 109, 34-38.	4.0	55
67	Two-Dimensional Nanomesh Arrays as Bifunctional Catalysts for N <sub>2</sub> Electrolysis. ACS Catalysis, 2020, 10, 11371-11379.	11.2	55
68	Dynamic Transformation between Covalent Organic Frameworks and Discrete Organic Cages. Journal of the American Chemical Society, 2020, 142, 21279-21284.	13.7	54
69	Efficient removal of methylene blue over composite-phase BiVO4 fabricated by hydrothermal control synthesis. Materials Chemistry and Physics, 2012, 136, 897-902.	4.0	52
70	Ultrathin two-dimensional π–d conjugated coordination polymer Co <sub>3</sub> (hexaaminobenzene) <sub>2</sub> nanosheets for highly efficient oxygen evolution. Journal of Materials Chemistry A, 2020, 8, 369-379.	10.3	50
71	Synthesis, characterization and enhanced gas sensing performance of WO3 nanotube bundles. New Journal of Chemistry, 2013, 37, 4241.	2.8	49
72	Graphene-based cobalt sulfide composite hydrogel with enhanced electrochemical properties for supercapacitors. New Journal of Chemistry, 2016, 40, 2843-2849.	2.8	49

#	Article	IF	CITATIONS
73	Effect of the counter ions on composition and morphology of bismuth oxyhalides and their photocatalytic performance. Chemical Engineering Journal, 2016, 299, 217-226.	12.7	48
74	The enhanced adhesion between overlong TiNxOy/MnO2 nanoarrays and Ti substrate: Towards flexible supercapacitors with high energy density and long service life. Nano Energy, 2018, 43, 91-102.	16.0	48
75	Spinel-type FeNi <sub>2</sub> S <sub>4</sub> with rich sulfur vacancies grown on reduced graphene oxide toward enhanced supercapacitive performance. Inorganic Chemistry Frontiers, 2021, 8, 2271-2279.	6.0	48
76	Synthesis of δ-Bi2O3 microflowers and nanosheets using CH3COO(BiO) self-sacrifice precursor. Materials Letters, 2016, 162, 218-221.	2.6	47
77	Synthesis of Unique Flowerlike Bi <sub>2</sub> O <sub>2</sub> (OH)(NO <sub>3</sub> ) Hierarchical Microstructures with High Surface Area and Superior Photocatalytic Performance. Chemistry - A European Journal, 2017, 23, 3891-3897.	3.3	47
78	A Facile Hydrothermal Synthesis of a MnCo2O4@Reduced Graphene Oxide Nanocomposite for Application in Supercapacitors. Chemistry Letters, 2014, 43, 83-85.	1.3	45
79	Two-dimensional transition metal diborides: promising Dirac electrocatalysts with large reaction regions toward efficient N <sub>2</sub> fixation. Journal of Materials Chemistry A, 2019, 7, 25887-25893.	10.3	45
80	Preparing Bi <sub>12</sub> SiO <sub>20</sub> crystals at low temperature through nontopotactic solid-state transformation and improving its photocatalytic activity by etching. Journal of Materials Chemistry A, 2015, 3, 7413-7421.	10.3	44
81	Controlled synthesis of bismuth-containing compounds (α-, β- and δ-Bi <sub>2</sub> O <sub>3</sub> ,) Tj ETQq1 and their photocatalytic performance. CrystEngComm. 2015. 17. 9185-9192.	1 0.78431 2.6	l4 rgBT /Ov€ 44
82	Hollow mesoporous carbon spheres enwrapped by small-sized and ultrathin nickel hydroxide nanosheets for high-performance hybrid supercapacitors. Journal of Power Sources, 2018, 402, 43-52.	7.8	44
83	Sustainable Electrosynthesis of Porous CuN <sub>3</sub> Films for Functional Energetic Chips. ACS Sustainable Chemistry and Engineering, 2020, 8, 3969-3975.	6.7	44
84	Band Engineering and Morphology Control of Oxygen-Incorporated Graphitic Carbon Nitride Porous Nanosheets for Highly Efficient Photocatalytic Hydrogen Evolution. Nano-Micro Letters, 2021, 13, 48.	27.0	43
85	Highly efficient removal of aqueous chromate and organic dyes by ultralong HCOOBiO nanowires. Chemical Engineering Journal, 2015, 262, 169-178.	12.7	42
86	Evidence of oxygen bubbles forming nanotube embryos in porous anodic oxides. Nanoscale Advances, 2021, 3, 4659-4668.	4.6	42
87	Catalytic hydrogenation of p-nitrophenol using a metal-free catalyst of porous crimped graphitic carbon nitride. Applied Surface Science, 2019, 480, 888-895.	6.1	41
88	Scalable synthesis of a foam-like FeS <sub>2</sub> nanostructure by a solution combustion–sulfurization process for high-capacity sodium-ion batteries. Nanoscale, 2019, 11, 178-184.	5.6	40
89	Carbon-Induced Generation of Hierarchical Structured Ni <sub>0.75</sub> Co <sub>0.25</sub> (CO <sub>3</sub> ) <sub>0.125</sub> (OH) <sub>2</sub> for Enhanced Supercapacitor Performance. ACS Applied Materials & Interfaces, 2017, 9, 44441-44451.	8.0	39
90	Labyrinth-inspired nitrogen-sulfur co-doped reduced holey graphene oxide/carbonized cellulose paper: A permselective and multifunctional interlayer for high-performance lithium-sulfur batteries. Journal of Power Sources, 2019, 434, 226728.	7.8	39

#	Article	IF	CITATIONS
91	Surface pore-containing NiCo2O4 nanobelts with preferred (311) plane supported on reduced graphene oxide: A high-performance anode material for lithium-ion batteries. Electrochimica Acta, 2018, 271, 137-145.	5.2	38
92	Preparation, electrochemical properties, and adsorption kinetics of Ni <sub>3</sub> S <sub>2</sub> /graphene nanocomposites using alkyldithiocarbonatio complexes of nickel( <scp>ii</scp> ) as single-source precursors. New Journal of Chemistry, 2013, 37, 654-662.	2.8	37
93	Biomass-derived C/N co-doped Ni(OH) <sub>2</sub> /Ni <sub>x</sub> S <sub>y</sub> with a sandwich structure for supercapacitors. Journal of Materials Chemistry A, 2018, 6, 17417-17425.	10.3	37
94	Synthesis of Bi2O3 architectures in DMF–H2O solution by precipitation method and their photocatalytic activity. Journal of Alloys and Compounds, 2014, 614, 353-359.	5.5	36
95	Recent advances in the heteroatom doping of perovskite oxides for efficient electrocatalytic reactions. Nanoscale, 2021, 13, 19840-19856.	5.6	36
96	Mesoporous transition metal oxides quasi-nanospheres with enhanced electrochemical properties for supercapacitor applications. Journal of Colloid and Interface Science, 2016, 483, 73-83.	9.4	35
97	Two basic bismuth nitrates: [Bi6O6(OH)2](NO3)4· 2H2O with superior photodegradation activity for rhodamine B and [Bi6O5(OH)3](NO3)5· 3H2O with ultrahigh adsorption capacity for methyl orange. Applied Surface Science, 2017, 422, 283-294.	6.1	35
98	Debunking the effect of water content on anodizing current: Evidence against the traditional dissolution theory. Electrochemistry Communications, 2020, 119, 106815.	4.7	35
99	Ultrafine silver nanoparticles obtained from ethylene glycol at room temperature: catalyzed by tungstate ions. Dalton Transactions, 2014, 43, 132-137.	3.3	34
100	Deposition of cocoon-like ZnO on graphene sheets for improving gas-sensing properties to ethanol. Applied Surface Science, 2015, 357, 1593-1600.	6.1	34
101	Hexagonal prism arrays constructed using ultrathin porous nanoflakes of carbon doped mixed-valence Co–Mn–Fe phosphides for ultrahigh areal capacitance and remarkable cycling stability. Journal of Materials Chemistry A, 2019, 7, 4431-4437.	10.3	34
102	Fe <sub>3</sub> O <sub>4</sub> -CoP <sub><i>x</i></sub> Nanoflowers Vertically Grown on TiN Nanoarrays as Efficient and Stable Electrocatalysts for Overall Water Splitting. ACS Applied Nano Materials, 2019, 2, 40-47.	5.0	34
103	Gas expansion-assisted preparation of 3D porous carbon nanosheet for high-performance sodium ion hybrid capacitor. Journal of Power Sources, 2020, 475, 228679.	7.8	34
104	Facet Engineering in Ultrathin Two-Dimensional NiFe Metal–Organic Frameworks by Coordination Modulation for Enhanced Electrocatalytic Water Oxidation. ACS Sustainable Chemistry and Engineering, 2021, 9, 10892-10901.	6.7	34
105	Task-Specific Synthesis of 3D Porous Carbon Nitrides from the Cycloaddition Reaction and Sequential Self-Assembly Strategy toward Photocatalytic Hydrogen Evolution. ACS Applied Materials & Interfaces, 2020, 12, 40433-40442.	8.0	33
106	Construction of N-doped carbon@MoSe2 core/branch nanostructure via simultaneous formation of core and branch for high-performance lithium-ion batteries. Electrochimica Acta, 2017, 256, 19-27.	5.2	32
107	Hierarchically Structured Twoâ€Dimensional Bimetallic CoNiâ€Hexaaminobenzene Coordination Polymers Derived from Co(OH) <sub>2</sub> for Enhanced Oxygen Evolution Catalysis. Small, 2020, 16, e1907043.	10.0	32
108	Batteryâ€Ðriven N <sub>2</sub> Electrolysis Enabled by Highâ€Entropy Catalysts: From Theoretical Prediction to Prototype Model. Small, 2022, 18, e2106358.	10.0	32

Јимwи Zни

#	Article	IF	CITATIONS
109	Room-temperature synthesis from molecular precursors and photocatalytic activities of ultralong Sb2S3 nanowires. RSC Advances, 2011, 1, 1364.	3.6	31
110	MXene-based porous and robust 2D/2D hybrid architectures with dispersed Li3Ti2(PO4)3 as superior anodes for lithium-ion battery. Chemical Engineering Journal, 2021, 405, 127049.	12.7	31
111	An ion exchange strategy to BiOI/CH3COO(BiO) heterojunction with enhanced visible-light photocatalytic activity. Applied Surface Science, 2017, 403, 103-111.	6.1	30
112	Three-dimensional nickel hydroxide/graphene composite hydrogels and their transformation to NiO/graphene composites for energy storage. Journal of Materials Chemistry A, 2015, 3, 21682-21689.	10.3	29
113	Well-dispersed ultrafine nitrogen-doped TiO 2 with polyvinylpyrrolidone (PVP) acted as N-source and stabilizer for water splitting. Journal of Energy Chemistry, 2016, 25, 1-9.	12.9	28
114	A facile and rapid room-temperature route to hierarchical bismuth oxyhalide solid solutions with composition-dependent photocatalytic activity. Journal of Colloid and Interface Science, 2016, 477, 25-33.	9.4	27
115	Quantitative Analysis of Oxide Growth During Ti Galvanostatic Anodization. Journal of the Electrochemical Society, 2020, 167, 113501.	2.9	27
116	Preparation and characterization of LaNiO3 nanocrystals. Materials Research Bulletin, 2006, 41, 1565-1570.	5.2	26
117	Synthesis of nanosheet-based hierarchical BiO2 microtubes and its photocatalytic performance. Applied Surface Science, 2018, 455, 616-621.	6.1	26
118	Great influence of a small amount of capping agents on the morphology of SnS particles using xanthate as precursor. Journal of Alloys and Compounds, 2011, 509, 2180-2185.	5.5	25
119	Phosphorous/oxygen co-doped mesoporous carbon bowls as sulfur host for high performance lithium-sulfur batteries. Journal of Power Sources, 2020, 450, 227658.	7.8	25
120	Two-Dimensional Molecular Sheets of Transition Metal Oxides toward Wearable Energy Storage. Accounts of Chemical Research, 2020, 53, 2443-2455.	15.6	25
121	Synthesis of egg-tart shaped Bi2O2CO3 hierarchical nanostructures from single precursor and its photocatalytic performance. Materials Letters, 2015, 138, 235-237.	2.6	24
122	Largeâ€Area Nanosphere Selfâ€Assembly Monolayers for Periodic Surface Nanostructures with Ultrasensitive and Spatially Uniform SERS Sensing. Small, 2022, 18, e2104202.	10.0	24
123	Rapid synthesis of ultrafine K2Ln2Ti3O10 (Ln=La, Nd, Sm, Gd, Dy) series and its photoactivity. Journal of Solid State Chemistry, 2005, 178, 761-768.	2.9	23
124	Solution-phase synthesis of Cu2O cubes using CuO as a precursor. Materials Letters, 2008, 62, 2081-2083.	2.6	23
125	Title is missing!. Journal of Materials Science Letters, 2003, 22, 253-255.	0.5	22
126	A convenient method for preparing shape-controlled nanocrystalline Cu2O in a polyol or water/polyol system. Powder Technology, 2008, 181, 249-254.	4.2	22

#	Article	IF	CITATIONS
127	An in situ oxidation route to fabricate graphene nanoplate–metal oxide composites. Journal of Solid State Chemistry, 2011, 184, 1393-1399.	2.9	22
128	High capacity supercapacitor material based on reduced graphene oxide loading mesoporpus murdochite-type Ni 6 MnO 8 nanospheres. Electrochimica Acta, 2016, 219, 284-294.	5.2	22
129	Stabilizing Layered Structure in Aqueous Electrolyte via Dynamic Water Intercalation/Deintercalation. Advanced Materials, 2022, 34, e2108541.	21.0	22
130	Facile solvothermal synthesis of graphene–MnOOH nanocomposites. Journal of Solid State Chemistry, 2010, 183, 2552-2557.	2.9	21
131	Facile Fabrication of Nanoparticles Confined in Graphene Films and Their Electrochemical Properties. Chemistry - A European Journal, 2013, 19, 7631-7636.	3.3	21
132	The construction of hierarchical hollow Double-Shelled Co3O4 for the enhanced thermal decomposition of Ammonium perchlorate. Applied Surface Science, 2022, 571, 151342.	6.1	21
133	Boosting Alkaline Hydrogen Evolution on Stoichiometric Molybdenum Carbonitride via an Interstitial Vacancyâ€Elimination Strategy. Advanced Energy Materials, 2022, 12, .	19.5	21
134	Beneficial restacking of 2D nanomaterials for electrocatalysis: a case of MoS <sub>2</sub> membranes. Chemical Communications, 2020, 56, 7005-7008.	4.1	20
135	Synthesis of Er2Ti2O7 nanocrystals and its electrochemical hydrogen storage behavior. Journal of Alloys and Compounds, 2009, 480, L45-L48.	5.5	19
136	One-pot synthesis of 3D hierarchical Bi 2 S 3 /(BiO) 2 CO 3 hollow microspheres at room temperature and their photocatalytic performance. Materials Chemistry and Physics, 2017, 187, 72-81.	4.0	19
137	PtRu alloy nanoparticles embedded on C2N nanosheets for efficient hydrogen evolution reaction in both acidic and alkaline solutions. Chemical Engineering Journal, 2022, 428, 131085.	12.7	19
138	Synthesis of α-Fe2O3 with the aid of graphene and its gas-sensing property to ethanol. Ceramics International, 2015, 41, 6978-6984.	4.8	18
139	CoSe <sub>2</sub> -Decorated NbSe <sub>2</sub> Nanosheets Fabricated via Cation Exchange for Li Storage. ACS Applied Materials & Interfaces, 2018, 10, 37773-37778.	8.0	18
140	Copper Azide Nanoparticleâ€Encapsulating MOFâ€Đerived Porous Carbon: Electrochemical Preparation for Highâ€Performance Primary Explosive Film. Small, 2022, 18, e2107364.	10.0	18
141	Regulating the transformation behavior of nickel iron metal–organic frameworks through a dual-ligand strategy for enhanced oxygen evolution reaction performance. Applied Surface Science, 2022, 592, 153252.	6.1	18
142	Dynamic Electrosorption Analysis as an Effective Means to Characterise the Structure of Bulk Graphene Assemblies. Chemistry - A European Journal, 2013, 19, 3082-3089.	3.3	17
143	A simple grinding-calcination approach to prepare the Co <sub>3</sub> O <sub>4</sub> –In <sub>2</sub> O <sub>3</sub> heterojunction structure with high-performance gas-sensing property toward ethanol. RSC Advances, 2016, 6, 105262-105269.	3.6	17
144	Ingenious construction of hierarchical spherical nanostructures by in-situ confining Ni–Co–Mn hydroxide nanosheets inside/outside hollow carbon nanospheres for high-performance hybrid supercapacitors. Journal of Energy Storage, 2021, 36, 102380.	8.1	17

#	Article	IF	CITATIONS
145	Precursor-modified strategy to synthesize thin porous amino-rich graphitic carbon nitride with enhanced photocatalytic degradation of RhB and hydrogen evolution performances. Chinese Journal of Catalysis, 2022, 43, 497-506.	14.0	16
146	Room-temperature synthesis of BiOCl and (BiO) 2 CO 3 with predominant {001} facets induced by urea and their photocatalytic performance. Journal of Environmental Chemical Engineering, 2017, 5, 987-994.	6.7	15
147	An in situ annealing route to [Bi6O6(OH)2](NO3)4·2H2O/g-C3N4 heterojunction and its visible-light-driven photocatalytic performance. Materials Research Bulletin, 2018, 101, 272-279.	5.2	15
148	General synthesis strategy for hollow porous prismatic graphitic carbon nitride: a high-performance photocatalyst for H2 production and degradation of RhB. Journal of Materials Science, 2020, 55, 6037-6050.	3.7	15
149	Hydrothermal ion exchange synthesis of CoM(M=Fe or Mn)/MXene 2D/2D hierarchal architectures for enhanced energy storage. Journal of Alloys and Compounds, 2022, 894, 162385.	5.5	15
150	A permselective and multifunctional 3D N-doped carbon nanotubes interlayer for high-performance lithium-sulfur batteries. Electrochimica Acta, 2022, 421, 140430.	5.2	15
151	Enhanced photo-electrochemical performances of graphene-based composite functionalized by Zn2+ tetraphenylporphyrin. Applied Surface Science, 2014, 321, 404-411.	6.1	14
152	Halogen-directed nucleation and growth of Bi 2 O 3 columnar hierarchitectures. Materials Research Bulletin, 2016, 76, 222-228.	5.2	14
153	One-step solvothermal synthesis of spherical spinel type NiFe2â^'xMnxO4-RGO as high-performance supercapacitor electrodes. Ceramics International, 2017, 43, 2226-2232.	4.8	14
154	Unique hollow-concave CoMoSx boxes with abundant mesoporous structure for high-performance hybrid supercapacitors. Electrochimica Acta, 2020, 337, 135824.	5.2	14
155	Dualâ€Ion Flux Management for Stable High Areal Capacity Lithium–Sulfur Batteries. Advanced Energy Materials, 2022, 12, .	19.5	14
156	Synthesis and characterization of BaCeO3 nanocrystals via solvothermal-based method. Journal of Rare Earths, 2008, 26, 51-54.	4.8	13
157	Morphology-controlled synthesis of ZnS nanostructures via single-source approaches. Materials Research Bulletin, 2010, 45, 813-817.	5.2	13
158	A facile solvent regulated method for phase control of two-dimensional nickel-cobalt hydroxide nanosheets: Towards improved performance hybrid supercapacitors. Materials Chemistry and Physics, 2018, 218, 172-181.	4.0	13
159	Millingâ€Induced Synthesis of BiOCl <sub>1â€<i>x</i></sub> Br <sub><i>x</i></sub> Solid Solution and Their Adsorptive and Photocatalytic Performance. Photochemistry and Photobiology, 2018, 94, 942-954.	2.5	12
160	Partial decomposition of NaBiO3 to δ-Bi2O3/NaBiO3 and α-Bi2O3/NaBiO3 heterojunctions in aqueous HAc solution respectively with good adsorption ability and photocatalytic performance. Materials Chemistry and Physics, 2019, 229, 6-14.	4.0	12
161	Growth Model of the Tin Anodizing Process and the Capacitive Performance of Porous Tin Oxides. Journal of Physical Chemistry C, 2020, 124, 3050-3058.	3.1	12
162	Loofah-like carbon nitride sponge towards the highly-efficient photocatalytic transfer hydrogenation of nitrophenols with water as the hydrogen source. Chemical Engineering Journal, 2022, 444, 136430.	12.7	12

#	Article	IF	CITATIONS
163	From understanding the formation mechanism to enhanced supercapacitor performance of VSB-5 with a hierarchical structure. Journal of Materials Chemistry A, 2017, 5, 16898-16906.	10.3	11
164	Metal-Cluster-Directed Surface Charge Manipulation of Two-Dimensional Nanomaterials for Efficient Urea Electrocatalytic Conversion. ACS Applied Nano Materials, 2018, 1, 6649-6655.	5.0	11
165	DFT coupled with NEGF study of the electronic properties and ballistic transport performances of 2D SbSiTe <sub>3</sub> . Nanoscale, 2020, 12, 9958-9963.	5.6	11
166	Fabrication of cubic Co3O4-hexagonal ZnO disk/rGO as a two-phase benzaldehyde sensor via a sequential nucleation strategy. Sensors and Actuators B: Chemical, 2021, 330, 129384.	7.8	11
167	Energetic properties of copper azide nanoparticles encapsulated within a conductive porous matrix via electrosynthesis. Chemical Engineering Journal, 2022, 450, 138131.	12.7	11
168	The facile synthesis of PbS cubes and Bi2S3 nanoflowers from molecular precursors at room temperature. Materials Letters, 2011, 65, 3344-3347.	2.6	10
169	Enhanced electrochemical properties of pseudocapacitor with Bi3.64Mo0.36O6.55 NPs as electrodes. Journal of Solid State Electrochemistry, 2017, 21, 403-408.	2.5	10
170	Grinding-assistant synthesis to basic bismuth nitrates and their photocatalytic properties. Materials Science in Semiconductor Processing, 2019, 101, 183-190.	4.0	10
171	Rotated angular modulated electronic and optical properties of bilayer phosphorene: A first-principles study. Applied Physics Letters, 2020, 117, .	3.3	10
172	One‣tep Synthesis of Bi <sub>2</sub> S <sub>3</sub> /BiOX and Bi <sub>2</sub> S <sub>3</sub> /(BiO) <sub>2</sub> CO <sub>3</sub> Heterojunction Photocatalysts by Using Aqueous Thiourea Solution as Both Solvent and Sulfur Source. ChemistrySelect, 2016, 1, 6136-6145.	1.5	9
173	Preparation of Copper-Embedded Graphene Nanocomposites for Catalytic Hydroxylation of Benzene to Phenol. Current Organic Chemistry, 2015, 18, 3136-3140.	1.6	9
174	Particle-based hematite crystallization is invariant to initial particle morphology. Proceedings of the National Academy of Sciences of the United States of America, 2022, 119, e2112679119.	7.1	9
175	A convenient method for preparing shape-controlled ZnO nanocrystals in a polyol/water mixture system without surfactants. Journal Wuhan University of Technology, Materials Science Edition, 2009, 24, 30-33.	1.0	8
176	Dynamic electrosorption analysis: a viable liquid-phase characterization method for porous carbon?. Journal of Materials Chemistry A, 2013, 1, 9332.	10.3	8
177	Ultrathin sheetlike BiOAc0.6710.33 solid solution with optimal energy levels and enhanced visible-light photocatalytic activity. Catalysis Communications, 2019, 119, 82-85.	3.3	8
178	Synthesis of CdS multipods from cadmium xanthate in ethylenediamine solution. Particuology, 2015, 19, 45-52.	3.6	7
179	Poly (triazine imide) ligand based 2D metal coordination polymers: Design, synthesis and application in electrocatalytic water oxidation. Electrochimica Acta, 2022, 401, 139463.	5.2	7
180	Microwave selective heating ultrafast construction of coral-like TiO2-MXene /graphene hybrid architectures for high-performance lithium-ion battery. Journal of Power Sources, 2022, 542, 231738.	7.8	7

#	Article	IF	CITATIONS
181	Fluorescent nucleotide-lanthanide nanoparticles for highly selective determination of picric acid. Mikrochimica Acta, 2021, 188, 18.	5.0	6
182	Molecular Examination of Ion-Pair Competition in Alkaline Aluminate Solutions Using In Situ Liquid SIMS. Analytical Chemistry, 2021, 93, 1068-1075.	6.5	6
183	Sacrificial Template Synthesis of Two-Dimensional Few-Layer MoSe <sub>2</sub> Coupled with Nitrogen-Doped Carbon Sheets for High-Performance Sodium Ion Hybrid Capacitors. ACS Applied Energy Materials, 2021, 4, 14735-14745.	5.1	6
184	Spontaneous growth of copper sulfide nanowires from elemental sulfur in carbon-coated Cu grids. Materials Letters, 2009, 63, 2358-2360.	2.6	5
185	Preparation and Characterization of Graphene Oxide-ZnO Nanocomposites. Materials Science Forum, 2011, 688, 228-232.	0.3	4
186	In situ assembly of Ag2O nanoparticles on low defect density carbon nanotubes. Materials Chemistry and Physics, 2012, 136, 666-672.	4.0	4
187	Covalently Induced Grafting of C <sub>2</sub> N Nanoflakes onto Reduced Graphene Oxide with Dominant Pseudocapacitive Behaviors for a High-Rate Sodium-Ion Battery Anode. ACS Sustainable Chemistry and Engineering, 2021, 9, 15946-15956.	6.7	4
188	Gradient Supramolecular Preorganization Endows the Derived N/P Dual-Doped Carbon Nanosheets with Tunable Storage Performance toward Sodium-Ion Batteries. Industrial & Engineering Chemistry Research, 2022, 61, 6997-7008.	3.7	4
189	Title is missing!. Journal of Materials Science Letters, 2003, 22, 931-933.	0.5	3
190	Preparation and characterization of poly(dimethyldiallyl ammonium)chloride and antiglobulin tests for antibody detection. Journal of Applied Polymer Science, 2003, 87, 1957-1961.	2.6	3
191	Preparation of novel structural nanosized Y2O3 powders and their catalytic activity on the decomposition of NH4ClO4. Reaction Kinetics and Catalysis Letters, 2007, 92, 247-256.	0.6	3
192	Self-assembly of (NH4)0.3TiO1.1F2.1 crystal by dinitrogen fixation as a precursor of N-doped TiO2 nanosheets. Journal of Nanoparticle Research, 2016, 18, 1.	1.9	3
193	Efficient Twoâ€Electron Oxygen Reduction to Hydrogen Peroxide Promoted by Agâ€7,7,8,8â€Tetracyanoquinodimethane Nanodots/Graphene Hydrogel Hybrid Electrocatalysts. ChemistrySelect, 2021, 6, 6450-6453.	1.5	3
194	Synthesis of visible light responsive ultrafine K4Ce2Nb10O30 by a stearic acid method. Journal of Rare Earths, 2009, 27, 811-814.	4.8	2
195	The Influence of Chain Length and Structure of Xanthates on the Morphology of Bi <sub>2</sub> S <sub>3</sub> Nanostructures. Nanoscience and Nanotechnology Letters, 2013, 5, 1030-1034.	0.4	1
196	A controllable synthetic route for preparing graphene-Cu and graphene-Cu2O nanocomposites using graphene oxide-Cuo as a precursor. Journal Wuhan University of Technology, Materials Science Edition, 2015, 30, 947-950.	1.0	1
197	Synthesis of CuO Nanocrystals in a Water-Isopropanol System. Advanced Materials Research, 2010, 148-149, 1011-1015.	0.3	0
198	Synthesis of rod-like ultrafine K4Ce2Nb10O30 via a salt-assistant stearic acid method. Journal of Rare Earths, 2011, 29, 664-667.	4.8	0

#	Article	IF	CITATIONS
199	KLn <sub>2</sub> Ti <sub>3</sub> O <sub>9·5</sub> (Ln = La, Nd, Sm, Gd, Dy): new family of layered perovskite oxides. Advances in Applied Ceramics, 2014, 113, 189-192.	1.1	0